JCTC Journal of Chemical Theory and Computation

Article

pubs.acs.org/JCTC

Structural and Electronic Properties of Photoexcited TiO_2 Nanoparticles from First Principles

Francesca Nunzi,*[,†,‡] Saurabh Agrawal,[†] Annabella Selloni,[§] and Filippo De Angelis*[,†]

[†]Computational Laboratory of Hybrid/Organic Photovoltaics (CLHYO), CNR-ISTM, via Elce di Sotto 8, I-06123 Perugia, Perugia, Italy

[‡]Dipartimento di Chimica, Biologia e Biotecnologie, Università degli Studi di Perugia, via Elce di Sotto 8, I-06123 Perugia, Perugia, Italy

[§]Department of Chemistry, Princeton University, Princeton, New Jersey 08544, United States

Supporting Information

ABSTRACT: The structure and energetics of excitons and individual electron and hole polarons in a model anatase TiO_2 nanoparticle (NP) are investigated by means of Density Functional Theory (DFT) and Time Dependent (TD)-DFT calculations. The effect of the Hartree−Fock exchange (HF-exc) contribution in the description of TiO_2 NPs with unpaired electrons is examined by comparing the results from semilocal and hybrid DFT functionals with different HF-exc percentages, including a long-range corrected hybrid functional. The performances of TD-DFT and ground state (SCF) DFT approaches in the description of the photoexcited polaron states in TiO_2 NPs are also analyzed. Our results confirm that the HF-exc contribution is essential to properly describe the self-trapping of the charge carriers. They also suggest that long-range corrected functionals are needed to properly describe excited state relaxation in TiO_2 NPs. TD-DFT geometry optimization of the lowest excited singlet and triplet states deliver photoluminescence values in close agreement with the experimental data.

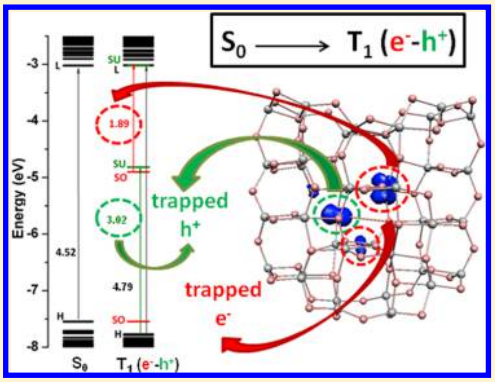

1. INTRODUCTION

The properties of photoexcited carriers are critical to the efficiency of TiO_2 in photocatalysis[1] and photovoltaics.[2] Upon photoexcitation by UV light absorption, valence band (VB) electrons of TiO_2 are promoted into unoccupied conduction band (CB) states, while correspondingly positively charged holes are created in the VB. The electron and hole charge carriers can diffuse to the surface and react with adsorbed molecules, or become trapped at defect sites, or again travel through the TiO_2 crystal to a collecting electrode. Electron−hole recombination usually represents a major competing process, so that higher quantum efficiency for the photocatalytic and photovoltaic processes can be attained by promoting charge separation and inhibiting subsequent recombination. Fundamental characterization of charge transport phenomena in TiO_2 is thus important for the development of models and the definition of strategies to control and reduce recombination rates. In this context, nanocrystalline anatase TiO_2 is usually preferred over rutile because it shows higher photocatalytic activity[3] and electron mobility,[4] thus allowing longer diffusion pathways of photogenerated carriers and increased quantum efficiencies.

Photogenerated charges in TiO_2 have been observed by electron paramagnetic resonance (EPR),[5] photoluminescence (PL),[6] and O_2 photodesorption.[7] PL measurements show a broad band centered at ∼2.3 eV attributed to radiative recombination of self-trapped excitons.[6e,8] The picture of the photoexcited electrons and holes is based on the polaron model,[9] in which the charge carriers become localized on just a few atoms, inducing a lattice distortion that stabilizes (traps) the localized state. The electrons are preferentially trapped at Ti sites to form Ti^{3+}ions, while holes are trapped by oxygen atoms to form O^- species, and both charge carriers can move from site to site through thermal hopping.

The accurate theoretical modeling of polaron states in TiO_2 has proven quite challenging. The self-interaction error of local and semilocal Density Functional Theory (DFT) functionals[10] results in an artificial bias toward delocalization of partially occupied states which reduces the Coulomb repulsion.[10] To mitigate the delocalization error and improve the description of the polaronic nature of excess electrons and holes in TiO_2, DFT+U methods[9,11] or hybrid functionals containing a fraction of exact Hartree−Fock exchange (HF-exc)[10b,12] are generally used. Among the latter, the Becke 3-parameter Lee−Yang−Parr (B3LYP) functional, originally fitted to reproduce molecular properties, has been shown to overcome many of the DFT deficiencies in the description of wide band gap semiconductors.[10a,13] For bulk anatase TiO_2, in particular, B3LYP calculations have predicted a self-trapping energy (ΔE_{trap}) of

Received: September 8, 2014
Published: January 14, 2015

DOI: 10.1021/ct500815x
J. Chem. Theory Comput. 2015, 11, 635−645

0.58 eV for the triplet exciton and ΔE_{trap} values of 0.23 and 0.74 eV for separated electron and hole polarons, respectively.[12]

Due to the prominent role of nanocrystalline TiO_2 in photocatalysis and photovoltaics, it is interesting to extend the investigation of polaron states to TiO_2 NPs. In this work, we characterize the structure and energetics of excitons and single electron and hole polarons in anatase TiO_2 NPs by means of hybrid DFT and Time Dependent (TD)-DFT calculations. TD-DFT offers a rigorous approach to the description of excited states and related optical transitions of fairly large systems, as the TiO_2 NPs studied here, and essentially represents the best compromise between accuracy and computational overhead. We focus on the effect of the HF-exc in the description of exciton and electron and hole polaron states by comparing the results of pure GGA and hybrid DFT functionals with different percentages of HF-exc. We also consider the range-separated exchange-correlation CAM-B3LYP functional,[14] which has proven successful in the TD-DFT scheme, especially for the description of excited states with a strong charge transfer character. Recent TD-DFT studies of the excited states of $(TiO_2)_n$ ($n < 13$) clusters[15] have shown that TD-B3LYP and TD-CAM-B3LYP yield results consistent with those of higher level Coupled-Cluster methods, whereas sizable discrepancies are found for pure GGA functionals. To model the TiO_2 NPs, we consider a stoichiometric $(TiO_2)_{38}$ cluster exposing majority (101) surfaces.[16] This model has been extensively characterized in previous theoretical studies[17−19] and shown to have electronic and optical properties comparable to those of periodic TiO_2 models.[20]

To describe the photoexcited NP, we consider both the lowest triplet (T_1) and singlet (S_1) excited states by TD-DFT, and for T_1 we also consider the lowest SCF triplet solution delivered by DFT. Photoluminescence measurements on anatase single crystals suggest T_1 to be the lowest excited state and to have a longer lifetime than the higher energy singlet excited state.[8,21] We further analyze the addition of a single excess electron or hole in the TiO_2 NP by considering a negatively/positively charged NP in an open-shell doublet (D_1) spin configuration. For all the considered electronic states, we allow the geometry to fully relax in the electronic state of interest, starting from the neutral TiO_2 NP ground state as initial structure. Similar calculations are performed also for a protonated $(TiO_2)_{38}$-H^+ cluster with H^+ bonded to a bridging two-coordinated oxygen (O_{2c}) atom. Specifically, we determine the ground (S_0) and lowest triplet (T_1) states of $(TiO_2)_{38}$-H^+, as well as the doublet (D_1) spin configuration of the $(TiO_2)_{38}$-H cluster with an excess electron.

Our results confirm some of the trends found for the bulk and the (101) surface of anatase.[12] With standard semilocal DFT (here the BLYP functional), excess electrons are delocalized over several Ti centers on the TiO_2 NP, and no energy level associated with singly occupied molecular orbitals (SOMOs) is present in the NP band gap. For an excess hole, instead, gap states from singly unoccupied molecular orbitals (SUMOs) appear also at the BLYP level at ∼0.48 eV above the valence band maximum, due to the presence of highly strained states in the NP. By employing hybrid functionals, both electrons and holes become more localized, and the SOMOs' and SUMOs' energy positions in the band gap depend on the amount of HF-exc. The self-trapping is always more pronounced for the holes, which have SUMO states with energy deeper in the band gap in comparison to electrons. The (e^--h^+) pair self-trapping energies predicted by the TD-DFT approach are smaller than those obtained by the hybrid SCF DFT approach.

2. COMPUTATIONAL DETAILS

All calculations were based on DFT and used both the generalized gradient approximation (GGA) with the BLYP[22] functional and three hybrid functionals, namely B3LYP-15,[23]B3LYP,[22b,23a] and CAM-B3LYP.[14] Additional TD-DFT calculations within the B3LYP and CAM-B3LYP functionals were employed to calculate the vertical (adiabatic) excitation energies of the lowest singlet (S_1) and triplet (T_1) excited states at the optimized geometry of the ground (excited) state. BLYP combines the gradient-corrected exchange functional of Becke[22a] with the Lee−Yang−Parr correlation functional[22b] (which also includes density gradient terms). B3LYP-15, as originally suggested by Reiher and co-workers,[24] is a reparametrized version of the B3LYP functional for the accurate estimation of energy differences between states of different spin. It contains a HF-exc percentage contribution of 15% in the exchange-correlation (XC) functional, to be compared to a value of 20% in the usual B3LYP functional. The latter provides a quite good description of the structural and electronic properties of oxide semiconductors,[10a,13] but is known to overestimate the spin-state splitting.[25] A smaller fraction of exact exchange (B3LYP-15) can overcome this problem. Range-separated exchange-correlation functionals are an alternative to the local/semilocal and conventional hybrid functionals for a better description of the charge transfer interaction. Among the long-range corrected hybrid functionals, we selected the Coulomb attenuated approximation, CAM-B3LYP, where the exchange term is splitted into short- and long-range components with a 19% and 65% of exact HF-exc contribution, respectively. In CAM-B3LYP the short-range exchange is therefore dominated by the local functional (DFT exchange), while the long-range is dominated by the exact exchange, thus improving the asymptotic behavior of the functional and allowing a better description of the charge transfer interactions in many cases where the B3LYP functional fails.

An all electron 6-31G(d) basis set was employed for all the calculations, and spin polarization was included for systems with unpaired electrons. Solvation effects of dimethylformamide (DMF), a common polar aprotic solvent with dielectric constant of 37, and water (for some selected electronic configurations) were included by means of the Conductor Polarizable Continuum Model (CPCM).[26]All the calculations have been performed using the Gaussian 09 program package.[27]

To model TiO_2 NPs, we used a $(TiO_2)_{38}$ cluster, obtained by appropriately "cutting" an anatase slab exposing the majority (101) surface.[16] Following the work by Persson et al.,[17] we consider a neutral stoichiometric TiO_2 cluster with no saturating atoms or groups at the edges,[18] which represents a good trade-off between accuracy and computational convenience and nicely reproduces the main electronic characteristics of TiO_2 NPs.[19] Geometry optimizations of the ground and (photo)excited states of $(TiO_2)_{38}$ were performed both in solvent and in vacuo (for some selected configurations) by considering the lowest energy closed-shell singlet (S_0) and open-shell triplet (T_1) spin configurations, respectively. Upon structural relaxation from the ground state geometry, the electron and hole in the triplet configuration become localized (trapped).[12]The relaxation or self-trapping energy (ΔE_{trap}) was calculated as the difference between the vertical $(S_0 \rightarrow T_1)_v$ and

DOI: 10.1021/ct500815x
J. Chem. Theory Comput. 2015, 11, 635−645

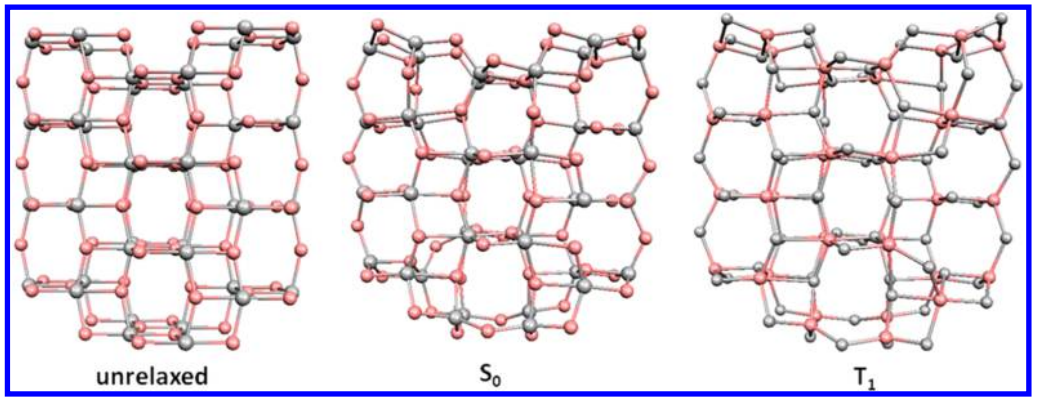

Figure 1. Unrelaxed, B3LYP-optimized ground state (S_0), and photoexcited state (T_1) geometries of the $(TiO_2)_{38}$ cluster. Titanium atoms in gray color and oxygen in pink.

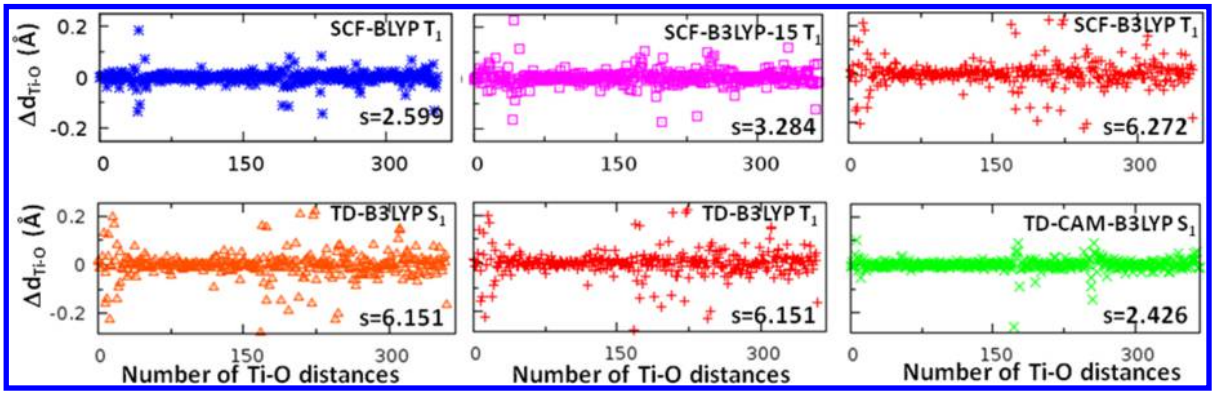

Figure 2. Differences between the Ti−O distances (Å) in the photoexcited state (e^--h^+, T_1/S_1) with respect to the ground state (S_0) for the $(TiO_2)_{38}$ cluster computed using ground state DFT (SCF, top of the panel) and TD-DFT (TD, bottom of the panel) with various functionals. For each excited state the standard deviation ($s{\cdot}10^2$) of Ti−O distances is also reported.

adiabatic $(S_0 \rightarrow T_1)_{ad}$ excitation energies for the ground state of the neutral cluster. Formally, ΔE_{trap} is an energetic measure of the structural differences between the ground and excited states of the cluster. In the case of an electron−hole pair (e^--h^+) created upon vertical photoexcitation, ΔE_{trap} represents the energy stabilization of the charge carriers upon structural relaxation. In a recent study,[28] similar calculations for the $(TiO_2)_{38}$ ground state within B3LYP and CAM-B3LYP, and the $(S_0 \rightarrow S_1)_v$ vertical excitation within TD-B3LYP and TD-CAMB3LYP have been already reported by one of the authors of the present work.

We further considered the addition of a single electron (e^-) and a single hole (h^+) separately on the $(TiO_2)_{38}$ NP, by performing geometry optimizations on the charged anion $(TiO_2)_{38}^-$ and cation $(TiO_2)_{38}^+$ clusters, respectively, in an open-shell doublet (D_1) spin configuration, starting from the geometry of the neutral $(TiO_2)_{38}$ ground state. As found for the T_1 state, the structural relaxation both stabilize and localize the charge carriers, allowing the evaluation of the relaxation or self-trapping energy (ΔE_{trap}) for a trapped electron and a trapped hole separately as the difference between the vertical $(S_0 \rightarrow D_1)_v$ and adiabatic $(S_0 \rightarrow D_1)_{ad}$ excitation energies. We note that for the TiO_2 cluster with one excess electron, the $(S_0 \rightarrow D_1)_v$ and $(S_0 \rightarrow D_1)_{ad}$ excitation energies correspond to the vertical and adiabatic electron affinity, denoted EA_v and EA_{ad}, respectively. Similarly, for the case of one excess hole on the TiO_2 cluster, the $(S_0 \rightarrow D_1)_v$ and $(S_0 \rightarrow D_1)_{ad}$ excitation energies correspond to the vertical and adiabatic ionization potential, denoted IP_v and IP_{ad}, respectively.

Lastly, we investigated the protonated NP, $(TiO_2)_{38}$-H^+cluster with an H^+ bonded to a bridging O_{2c} atom, in the closed shell (S_0) ground state and in the open-shell triplet (T_1) excited state. We also considered a single excess electron, which was described by the neutral $(TiO_2)_{38}$-H in a doublet (D_1) spin configuration. The geometries of these excited states were fully relaxed by considering the $(TiO_2)_{38}$-H^+cluster in the S_0 ground state as initial configuration.

3. RESULTS AND DISCUSSION

3.1. Structural Properties. The optimized molecular structures and main geometrical parameters for the considered systems are reported in Figure 1 and Table S1, Supporting Information. The $(TiO_2)_{38}$ ground state has been extensively investigated in previous studies using the B3LYP functional and different basis sets.[17−19,29] In agreement with those studies,[17−19,29] we found that the cluster geometry relaxation of neutral $(TiO_2)_{38}$ causes a decrease of the average Ti−O bond length, $(Ti-O)_{av}$, with respect to the truncated bulk structure (1.946 Å), due to the higher surface-to-bulk ratio in the cluster. We found $(Ti-O)_{av}$ lengths of 1.932, 1.912, 1.911, and 1.898 Å with the BLYP, B3LYP-15, B3LYP, and CAM-B3LYP functionals, respectively. Thus, hybrid functionals predict a more pronounced decrease of the $(Ti-O)_{av}$ length (0.04−0.05 Å) in comparison to the pure GGA functional (0.02 Å, see Table S1).

The geometry of the $(TiO_2)_{38}$ cluster in the photoexcited T_1 state and in the D_1 states with an excess electron/hole were optimized using the BLYP, B3LYP-15, and B3LYP functionals. It is known from previous studies[12] that the formation of the

DOI: 10.1021/ct500815x
J. Chem. Theory Comput. 2015, 11, 635−645

polaron in the bulk and (101) surface of anatase causes a reorganization of the local geometry around the Ti^{3+} and O^- sites. To better visualize the geometry reorganization upon excitation, here we plot the differences between the Ti−O bond distances in the excited state and in the ground state, positive and negative values corresponding to lengthening and shortening of the Ti−O distances upon excitation, respectively (see Figures 2 and S1−S3 in the Supporting Information).

At the B3LYP level, our calculations show a significant geometry reorganization both for the SCF T_1 (e^--h^+) and the single D_1 (e^-/h^+) photoexcited states, with computed differences of the Ti−O bond distances within 0.2 Å. The GGA BLYP functional predicts a less pronounced reorganization, especially for the reduced $(TiO_2)_{38}^-$ cluster, for which the changes of Ti−O distances do not exceed 0.07 Å with respect to S_0. With B3LYP-15, the computed Ti−O differences are within 0.1 Å for the reduced $(TiO_2)_{38}^-$ cluster and 0.2 Å for the cation $(TiO_2)_{38}^+$ and photoexcited (e^--h^+) clusters. For the T_1 (e^--h^+) photoexcited state, we optimized the geometry also at the CAM-B3LYP level and found Ti−O bond distance differences within 0.2 Å, i.e. very similar to those obtained with B3LYP.

We further considered the Ti−O distance differences between the S_0 ground state and the S_1 and T_1 excited states computed by TD-DFT, see Figure 2. We note that the geometrical relaxations in the TD-B3LYP S_1 and T_1 excited states are very similar, while the relaxation of S_1 with respect to S_0 given by TD-B3LYP is somewhat larger than that predicted by TD-CAM-B3LYP. Moreover, significant differences appear when comparing SCF T_1 and TD−DFT S_1 excited state geometries computed by CAM-B3LYP. These differences affect also the calculation of the adiabatic excitation energy and self-trapping energy, see below.

In summary, the results in Figures 2 and S1−S2 show that the level of structural reorganization upon photoexcitation depends significantly on the electronic structure method used. The changes of Ti−O distances for the photoexcited T_1 (e^--h^+) and D_1 (e^-) states of the protonated $(TiO_2)_{38}H^+$ cluster relative to the $(TiO_2)_{38}H^+$ ground state are reported in Figure S3, Supporting Information. These differences do not exceed 0.2 and 0.1 Å, respectively, at the B3LYP level of theory.

3.2. Electronic Properties. We analyzed the ground and excited state electronic properties of the $(TiO_2)_{38}$ and $(TiO_2)_{38}H^+$ clusters in terms of orbital energies, energy gaps, electron spin density distribution, and self-trapping energies. The results are reported in Tables 1 and 2 (Tables S2−S4, Supporting Information) and Figures 3−7 (Figures S4−S6, Supporting Information).

Table 1. Energy Gaps (in eV) for $(TiO_2)_{38}$ Computed at Various Levels of Theory in DMF Solution Evaluated as (i) One-Electron Kohn-Sham Eigenvalues HOMO and LUMO Difference ($\Delta E_{H\text{-}L}$), (ii) Energy Difference between the Vertical Ionization Potential $(IP)_v$ and Electron Affinity $(AE)_v$, and (iii) Vertical Excitation Energy $(S_0{\rightarrow}T_1)_v$. The Exciton Shift Values (ΔE_{ex}) Are Also Shown.

	BLYP	B3LYP-15	B3LYP	CAM-B3LYP
$\Delta E_{H\text{-}L}$	2.647	4.038	4.525	7.540
$(IP)_v$-$(EA)_v$	3.264	3.915	4.320	
$(S_0{\rightarrow}T_1)_v$	2.793	3.636	3.872	4.644
ΔE_{ex}	0.471	0.279	0.448	

Table 2. Lowest Vertical, $(S_0{\rightarrow}S_1)_v$ or $(S_0{\rightarrow}T_1)_v$, and Adiabatic, $(S_0{\rightarrow}S_1)_{ad}$ or $(S_0{\rightarrow}T_1)_{ad}$, TD-DFT Excitation Energies and Trapping Energies (ΔE_{trap}) for Different Photoexcited State (S_1 or T_1) of the $(TiO_2)_{38}$ Cluster Computed at Various Levels of Theory in DMF Solvent[a]

	$(S_0{\rightarrow}S_1)_v$	$(S_0{\rightarrow}S_1)_{ad}$	ΔE_{trap}	$(S_0{\rightarrow}T_1)_v$	$(S_0{\rightarrow}T_1)_{ad}$	ΔE_{trap}
TD-B3LYP	3.800	2.942	0.858	3.762	2.958	0.804
TD-CAM-B3LYP	4.425	3.918	0.507			

[a]Energies in eV.

Band Gap Energies. It is useful to recall that there are two different ways to determine the band gap. The electronic band gap, as measured by photoemission experiments, involves a change in the total number of electrons (i.e., ionized states), and it can be expressed in terms of single-particle energies. The optical band gap is related to light absorption experiments, and as such it involves the creation of an electron−hole excitonic pair. In general, the optical band gap is lower than the electronic band gap, because the electron and hole remain electrostatically bound in the excited state, lowering the state total energy. A standard way to evaluate the electronic band gap is through the difference between the LUMO and HOMO one-electron Kohn−Sham eigenvalues in the S_0 ground state ($\Delta E_{H\text{-}L}$ in Table 1). This orbital energy gap is only a crude estimate of the band gap, the quality of the approximation being determined by the computational approach used.[30] A more accurate estimate of the electronic band gap can be obtained through the energy difference between the vertical ionization potential $(IP)_v$ and electron affinity $(EA)_v$, which are given by the vertical excitation energies of the single excess hole, $(S_0{\rightarrow}D_1)_v^h$, and single excess electron, $(S_0{\rightarrow}D_1)_v^e$, respectively ($(IP)_v$-$(EA)_v$ in Table 1). On the other hand, the optical band gap can be estimated by considering the vertical excitation energy $(S_0{\rightarrow}T_1)_v$ or $(S_0{\rightarrow}S_1)_v$ of the photoexcited electron−hole pair, see Table 1. The energy difference between the electronic band gap, evaluated as $(IP)_v$-$(EA)_v$, and the optical band gap, evaluated as $(S_0{\rightarrow}T_1)_v$, provides an estimate of the electrostatic electron−hole interaction and is usually referred to as exciton shift (ΔE_{ex}, in Table 1).

Energy gaps calculated according to the definitions above are reported in Tables 1 and 2. Starting with the HOMO−LUMO gap, the BLYP functional yields a value $\Delta E_{H\text{-}L}$ = 2.65 eV, the hybrid B3LYP-15 and B3LYP functionals predict a larger band gap of 4.04 and 4.52 eV (4.53 eV in water solution, see Table S3, Supporting Information), respectively, whereas CAM-B3LYP yields an unreasonably large value of 7.54 eV, consistent with a previous study by one of us.[28] For the $(IP)_v$-$(EA)_v$ energy difference, instead, the BLYP computed value is 3.26 eV, i.e. 0.62 eV higher than the corresponding HOMO−LUMO gap, whereas the values predicted by the hybrid functionals are ∼0.2 eV smaller than the corresponding HOMO−LUMO gaps. As a result, $(IP)_v$-$(EA)_v$ values show smaller differences among various DFT functionals than those found for $\Delta E_{H\text{-}L}$.

As expected, the computed optical band gaps are always smaller than the electronic band gaps. In particular, the exciton shift (ΔE_{ex}) is 0.47, 0.28, and 0.45 eV when calculated at the BLYP, B3LYP-15, and B3LYP level of theory, respectively. It is interesting to notice that BLYP and B3LYP predict very similar values of ΔE_{ex}, suggesting an (e^--h^+) interaction of the same importance, whereas the computed exciton shift is smaller (by

DOI: 10.1021/ct500815x
J. Chem. Theory Comput. 2015, 11, 635−645

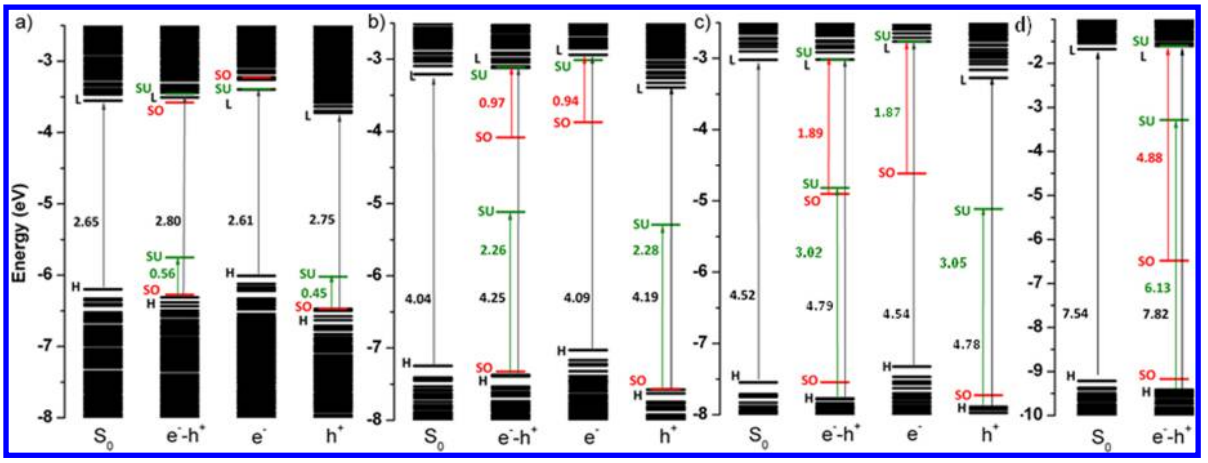

Figure 3. MOs energy level diagram for the $(TiO_2)_{38}$ cluster in the T_1 (e^--h^+), D_1 (e^-), and D_1 (h^+) states computed at various level of theory in DMF solvent: a) BLYP; b) B3LYP-15; c) B3LYP; d) CAM-B3LYP. HOMO and LUMO (H and L) are shown in black, while SOMOs and SUMOs (SO and SU) are shown in red and green, respectively; energy values in black refer to the $\Delta E_{H\text{-}L}$ energy gap, while values in red and green refer to the $\Delta E_{SO\text{-}L}$ and $\Delta E_{H\text{-}SU}$ energy gaps, respectively. See also Table S2 in the Supporting Information for a complete list of the MOs energy values.

0.17−0.19 eV) at the B3LYP-15 level. The large ΔE_{ex} predicted by BLYP originates from the high value of the $(IP)_v$-$(EA)_v$ gap, which can be considered as an error compensation effect. Further calculations of the optical band gap at the TD-B3LYP (TD-CAM-B3LYP) levels yield $(S_0 \rightarrow S_1)_v$ = 3.80 (4.42) eV, with an oscillator strength of 0.0016 (0.0041). The low intensity computed for the oscillator strength confirms the optically symmetry forbidden character of the electronic transition from the ground to the first excited state of singlet, as expected for an indirect band gap semiconductor. The agreement of the TD-B3LYP result with the experimental gap for bulk anatase (3.20 eV)[31] is quite good, considering the small size of the $(TiO_2)_{38}$ cluster. We also note the close similarity of the SCF-B3LYP and TD-B3LYP values for $(S_0 \rightarrow T_1)_v$, as well as the similarity of the TD-B3LYP values for the singlet, $(S_0 \rightarrow S_1)_v$, and triplet, $(S_0 \rightarrow T_1)_v$, vertical excitations.

Molecular Orbital Diagram. The Molecular Orbital (MO) energy level diagram for the TiO_2 NP (Figures 3 and S4−S6 and Tables S2−S3 in the Supporting Information) shows that upon excitation the charge carriers are trapped in energy levels inside the band gap, and the energy position of these levels depends strongly on the method employed for the calculations. In the photoexcited T_1 (e^--h^+) state, the high-energy SOMO of the trapped electron lies almost at the bottom of the unoccupied states with BLYP ($\Delta E_{SO\text{-}L}$ = 0.07 eV), while its energy is 0.97, 1.89, and even 4.88 eV below the LUMO with the B3LYP-15, B3LYP, and CAM-B3LYP methods, respectively. Similarly, the low-energy SUMO, representing the trapped hole, lies 0.56 eV above the occupied states at the BLYP level, while it is very deep in the gap with the hybrid functionals (2.26, 3.02, and 6.13 eV above the HOMO with the B3LYP-15, B3LYP, and CAM-B3LYP methods, respectively).

Similar results are found also for the TiO_2 NP with an excess electron or hole. For the reduced cluster, the highest SOMO is erroneously predicted to be inside the conduction band (0.17 eV from the LUMO) by BLYP. Thus, the GGA approach yields unphysical results for the energetic states associated with the excited electron, while the introduction of the exact HF-exc allows the localization of the trapped carriers states inside the band gap, with the holes placed deeper than the electrons at all the levels of theory. The MO diagram in Figure 3 confirms that BLYP tends to delocalize the electronic states, while hybrid functionals allow the description of spin-unpaired localized states in the band gap. In particular, B3LYP predicts the SOMOs to be 1.89 eV below the LUMO and 0.27 eV above the HOMO for the photoexcited T_1 (e^--h^+) TiO_2 cluster, 1.87 eV below the LUMO for a single excess electron, and 0.16 eV above the HOMO for a single excess hole.

Results for the protonated TiO_2 NP are reported in Figure S4 of the Supporting Information. $(TiO_2)_{38}H^+$ has a ground (S_0) state HOMO−LUMO energy gap of 4.59 eV at the B3LYP level, similar to that of the neutral, nonprotonated, system. In the T_1 spin state, the high energy SOMO is located 2.05 eV below the LUMO and the low energy SUMO at 2.71 eV above the HOMO. The single excess electron on the $(TiO_2)_{38}H^+$ confirms this picture, with a SOMO lying at 2.03 eV below the LUMO. A comparison with the MOs energy of the $(TiO_2)_{38}$ cluster, see Figures 3 and S4 in the Supporting Information, suggests that the protonated NP traps electrons more efficiently than the bare particle.

Spin Densities. Figure 4 shows the electron spin densities for the TiO_2 NP with photoexcited/excess electron and holes. For the T_1 state, the BLYP functional gives a spin density centered on three Ti sites (3d atomic orbitals on Ti36, Ti6, and Ti29; see Figure S7 in the Supporting Information for atom number labeling) and three O centers (2p atomic orbitals on O94, O113, and O49). The hybrid B3LYP-15 functional predicts almost the same spin localization on the O centers, while for the Ti centers there is a stronger localization on Ti36 vs Ti6. At the B3LYP and CAM-B3LYP levels the T_1 state shows strongly localized electrons and holes at Ti3 and O51, respectively (thus sites different from those found with the other functionals). Similarly, for an excess electron, the BLYP spin density is shared by three Ti centers, the B3LYP-15 functional localizes the spin density mainly on a single Ti center (Ti36) with a minor contribution on Ti6, while B3LYP localizes the electron exclusively on the Ti3 center. The excess hole is partially delocalized on three O centers (O94, O113, and O49) at the BLYP and B3LYP-15 levels, which predicts however a stronger contribution on the O94 atom. As found for the T_1 solution, the excess hole is localized in a completely different region at the B3LYP level, viz. on the O51 atom, with a small contribution from O70 and O79.

DOI: 10.1021/ct500815x
J. Chem. Theory Comput. 2015, 11, 635−645

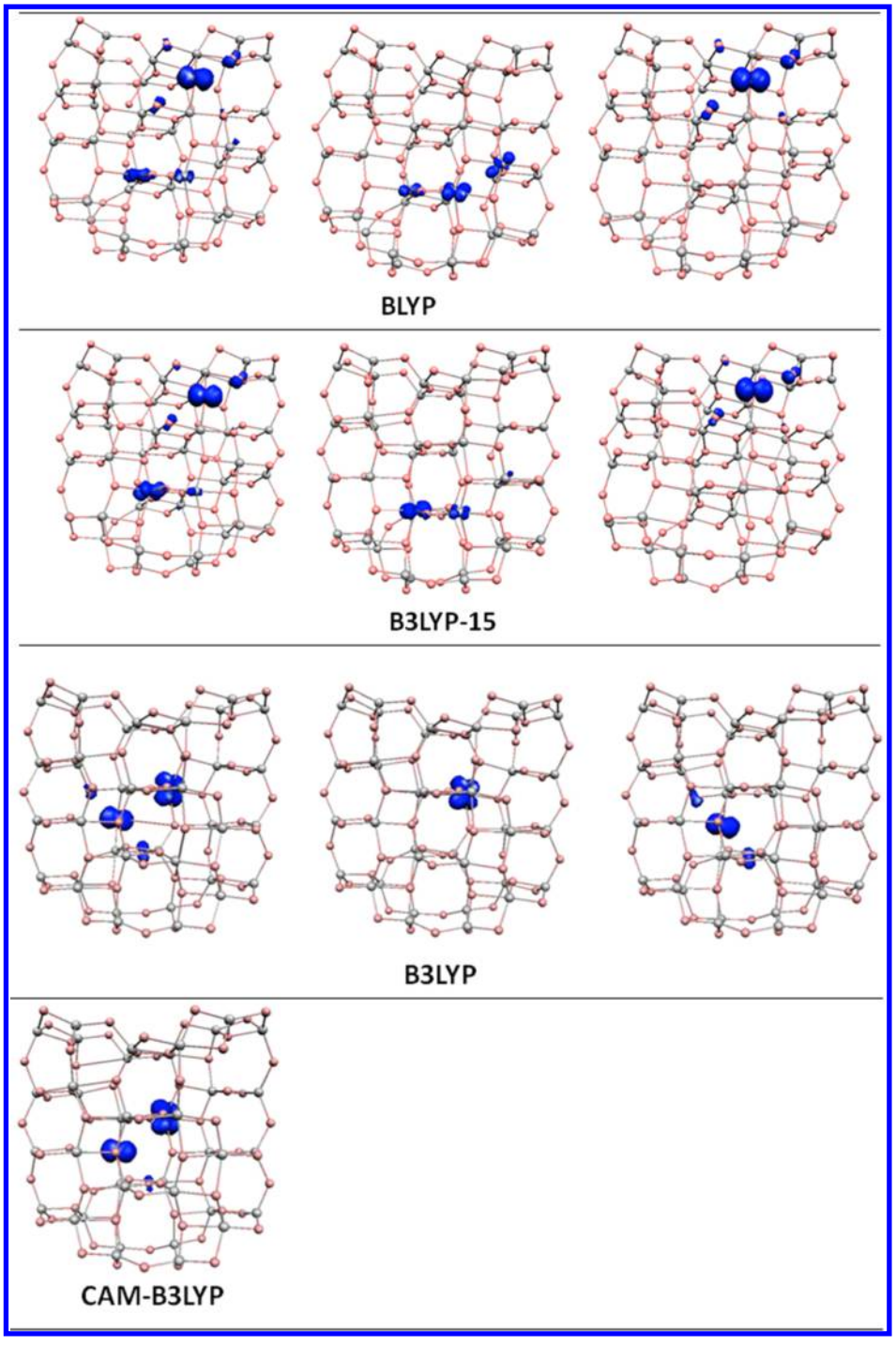

Figure 4. Electron spin densities (isovalue = 0.02 e·au^{-3}) computed at various levels of theory in DMF solvent for the photoexcited T_1 (e^--h^+) state (left), single extra electron D_1 (e^-) (middle) and single extra hole D_1 (h^+) (right) in the $(TiO_2)_{38}$ cluster.

From these results we can see that the spin density of the photoexcited cluster corresponds closely to the sum of the spin densities of the single excess electron and hole, the degree of spin density localization increasing with the increase of the HF-exc fraction. It also appears that the excess hole prefers to localize on undercoordinated O_{2c} rather than on fully coordinated O_{3c} centers (at all levels of theory). By contrast, rather than localizing on one of the undercoordinated Ti_{4c} sites, as one would intuitively expect, the excess electron appears to prefer a fully coordinated Ti_{6c} center (Ti51 with B3LYP and CAM-B3LYP and Ti36 at all the other levels of theory). This may be attributed to the fact that, upon geometry optimization of the NP from the bulk structure, the Ti_{4c} centers are enforced to strongly rearrange from an octahedral to a tetragonal configuration, with a sizable shortening (0.1−0.2 Å at the B3LYP level) of the Ti−O bond distances, while the Ti_{6c} centers, keeping an almost unaltered octahedral configuration, undergo only slight lengthening of Ti−O bonds. On the other hand, the preference of the excess electron for the Ti51 or Ti36 centers among the four Ti_{6c} present on the $(TiO_2)_{38}$ NP is likely due to the asymmetry of our model.

DOI: 10.1021/ct500815x
J. Chem. Theory Comput. 2015, 11, 635−645

Table 3. Lowest Vertical, $(S_0 \rightarrow T_1)_v$ or $(S_0 \rightarrow D_1)_v$, and Adiabatic, $(S_0 \rightarrow T_1)_{ad}$ or $(S_0 \rightarrow D_1)_{ad}$, SCF Excitation Energies and Trapping Energies (ΔE_{trap}) for Different Electronic Configurations (See Text for Labeling) of the $(TiO_2)_{38}$ and $(TiO_2)_{38}H^+$ Clusters Computed at Various Levels of Theory in DMF Solvent[a]

	T_1 (e^--h^+)			D_1 (e^-)			D_1 (h^+)		
$(TiO_2)_{38}$	$(S_0 \rightarrow T_1)_v$	$(S_0 \rightarrow T_1)_{ad}$	ΔE_{trap}	$(S_0 \rightarrow D_1)_v$	$(S_0 \rightarrow D_1)_{ad}$	ΔE_{trap}	$(S_0 \rightarrow D_1)_v$	$(S_0 \rightarrow D_1)_{ad}$	ΔE_{trap}
BLYP	2.793	2.470	0.323	−3.157	−3.327	0.169	6.421	6.144	0.307
B3LYP-15	3.636	2.742	0.894	−3.274	−3.451	0.177	7.189	6.388	0.800
B3LYP	3.872	2.502	1.369	−3.190	−3.751	0.561	7.510	6.511	0.999
CAM-B3LYP	4.644	2.434	2.210						
$(TiO_2)_{38}H^+$									
B3LYP	3.814	2.601	1.213	−3.477	−4.123	0.647			

[a]Energies in eV.

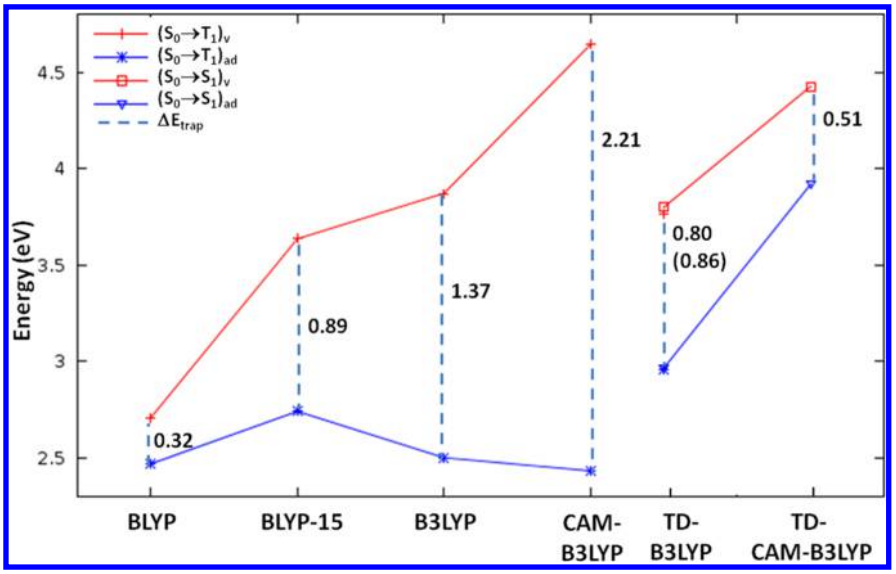

Figure 5. Lowest triplet/singlet vertical (red) and adiabatic (blue) excitation energies computed at various level of theory. The computed self-trapping energies (dashed lines) are also given (black values). All energies in eV.

Results for the protonated NP are also in this case reported in the Supporting Information. The photoexcited (T_1) state shows a different spin density distribution with respect to the deprotonated NP at the same B3LYP level of theory. As shown in Figure S6, the (e^--h^+) pair is mainly localized in proximity of the proton (on Ti37 and O108, being six- and two-coordinated, respectively). Similarly, the doublet spin configuration for the NP with an extra electron shows that the electron becomes trapped on the Ti37 (six-coordinated) center near the proton.

Self-Trapping Energies. Tables 2 and 3, Figure 5, and Tables S4−S5 in the Supporting Information show the lowest vertical, $(S_0 \rightarrow D_1)_v$, and adiabatic, $(S_0 \rightarrow D_1)_{ad}$, SCF excitation energies and trapping energies (ΔE_{trap}) for the $(TiO_2)_{38}$ and $(TiO_2)_{38}H^+$ clusters computed at different levels of theory. Since the spin densities in Figure 4 suggest different photoexcited electronic configurations at different levels of theory, we also performed test calculations in which the same functional was applied to different geometrical structures, and, vice versa, the same optimized structure was calculated with different functionals. The results of these tests (see Table S6 and Figures S8 and S9 in the Supporting Information) show that trends in the computed excitation and trapping energies are not significantly affected by the apparent differences in the electronic configurations.

From Table 3 and Figure 5, we can see that, not surprisingly, the computed ΔE_{trap} values increase with the increase of the HF-exc percentage. For the photoexcited $(TiO_2)_{38}$ NP, in particular, ΔE_{trap} values of 0.32, 0.89, 1.37, and 2.21 eV are obtained with the BLYP, B3LYP-15, B3LYP, and CAM-B3LYP functionals, respectively. The large stabilization (2.21 eV), predicted by CAM-B3LYP, can be attributed to the increased HF-exc at long-range.

Table 3 also shows that at all the levels of theory ΔE_{trap} is much larger for holes than for electrons. This trend correlates with the MOs energy level diagram (Figure 3), where the SUMO states related to trapped holes are deeper in the gap in comparison to the SOMO states of trapped electrons. The difference between electron and hole self-trapping energies is relatively small, 0.17 vs 0.31 eV, at the GGA level, but becomes significantly more pronounced with hybrid functionals, 0.18 vs 0.80 eV with B3LYP-15, and 0.56 vs 1.00 eV with B3LYP. Interestingly, if we compare the sum of the individual e^-/h^+ contributions to the (e^--h^+) pair trapping energies, we can see that the former is larger by ca. 0.1−0.2 eV, thus suggesting that some interaction, decreasing the electron−hole pair self-trapping energy, occurs between the carriers in the photo-excited state.

We also evaluated the effect of the DMF solvent environment on the carrier trapping energies by carrying out selected B3LYP calculations both in vacuo and in water solvent (see Tables S4 and S5 in the Supporting Information). Computed values of ΔE_{trap} are higher in vacuo, i.e. 1.50, 0.67, and 0.70 eV,

DOI: 10.1021/ct500815x
J. Chem. Theory Comput. 2015, 11, 635−645

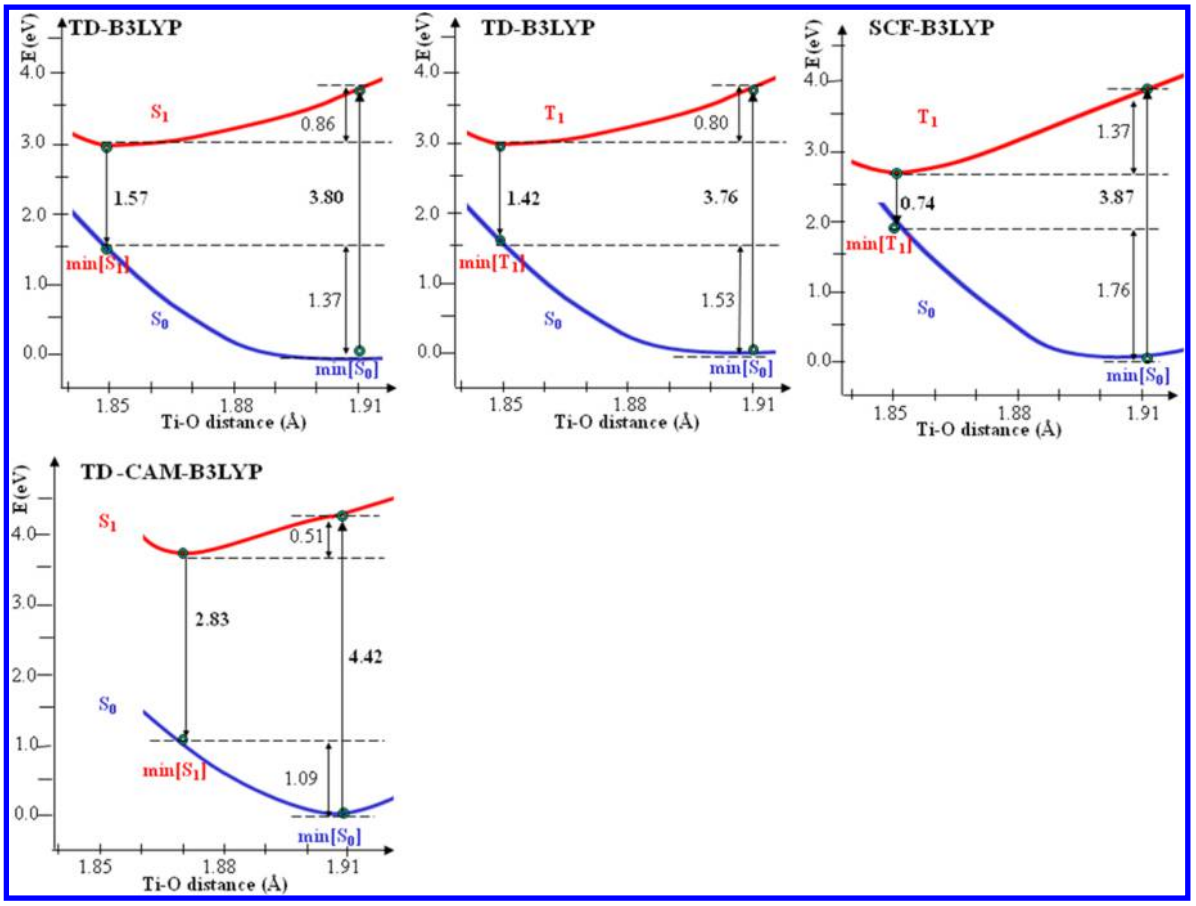

Figure 6. Schematic representation of the potential energy surfaces for the ground and first photoexcited state (S_1 or T_1) computed using ground state DFT (SCF) and TD-DFT (TD) with the B3LYP (top of the panel) and CAM-B3LYP (bottom of the panel) functionals. The average of the optimized Ti−O distances for the $(TiO_2)_{38}$ cluster was used as reaction coordinate to define the S_0 minimum, while the displacement of each excited state minimum from the ground state minimum was estimated from the corresponding standard deviation, given in Figure 2.

for the photoexcited T_1 (e^--h^+), excess electron e^-, and excess hole h^+, respectively. It is worth noting that the self-trapping energies of electron and hole polarons are very similar in vacuo, whereas ΔE_{trap} is 0.3−0.4 eV larger for the hole in both DMF and water solvents. By comparing the MOs diagram for the electron and hole polaron states in vacuo (water/DMF solvent), it also appears that the SOMO lies at 1.85 (1.94/1.87) eV below the LUMO and the SUMO at 2.70 (2.80/3.05) eV above the HOMO, respectively, see Figures 3 and S5 in the Supporting Information, i.e. the MOs for the trapped electron and hole are almost at the same energy inside the gap in vacuo, water, and DMF solvent. As a result of solvation, however, the *absolute* energies of the electron and hole polaron states in DMF and water solvent differ by a few eV with respect to results in vacuo (see Figure S4 in the Supporting Information). Altogether, our results indicate that the use of different solvents, notably water vs DMF, does not affect substantially neither the self-trapping energies of electron and hole polarons nor the MOs' energies within the NP band gap.

A remarkable feature of the results in Tables 2 and 3 and Figure 5 is that the (e^--h^+) pair self-trapping energies predicted by the TD-DFT approach are much smaller than those obtained by the hybrid SCF DFT approach. We found ΔE_{trap} = 0.80 (0.86) eV for the photoexcited state in the T_1 (S_1) state at the TD-B3LYP level, while a lower value (0.51 eV) was obtained for S_1 at the TD-CAM-B3LYP level. We also determined the lowest triplet excited state at the TD-B3LYP level using the T_1 SCF-B3LYP optimized geometry. This gave a value of 3.19 eV for the ($S_0 \rightarrow T_1$) adiabatic excitation energy, with a self-trapping energy of 0.68 eV, to be compared to ΔE_{trap} = 1.37 eV at the SCF-B3LYP level. This shows that the TD self-trapping energy is much smaller than the SCF one, even when the SCF optimized geometry is employed. Therefore, the difference in the ΔE_{trap} values at the SCF and TD level of theory cannot be simply related to the different geometry.

A visual representation of the Franck−Condon (FC) diagram inferred from the above results is shown in Figure 6. The FC diagram highlights also the emission energies from the equilibrium geometry of the excited state to the distorted geometry in the ground state. While the SCF approach predicts quite low emission energies (~0.7 eV), the TD-DFT results deliver energy values between 1.42 and 2.83 eV, much closer to the observed PL peak (~2.3 eV) from the radiative recombination of self-trapped excitons.[6e,8]

To clarify the origin of the discrepancy between the SCF and TD-DFT self-trapping energy values, we analyzed the electron density differences between excited and ground states computed by TD-DFT at the B3LYP and CAM-B3LYP, see Figure 7. The electron density difference for the singlet excited state shows that upon relaxation the excited electron and hole become localized on one Ti_{6c} (3 and 32 at the B3LYP and CAM-B3LYP level, respectively) and one O_{2c} (51 at B3LYP and CAM-B3LYP level) in close proximity, thus suggesting a low charge transfer character of the excitation. The electron

DOI: 10.1021/ct500815x
J. Chem. Theory Comput. 2015, 11, 635−645

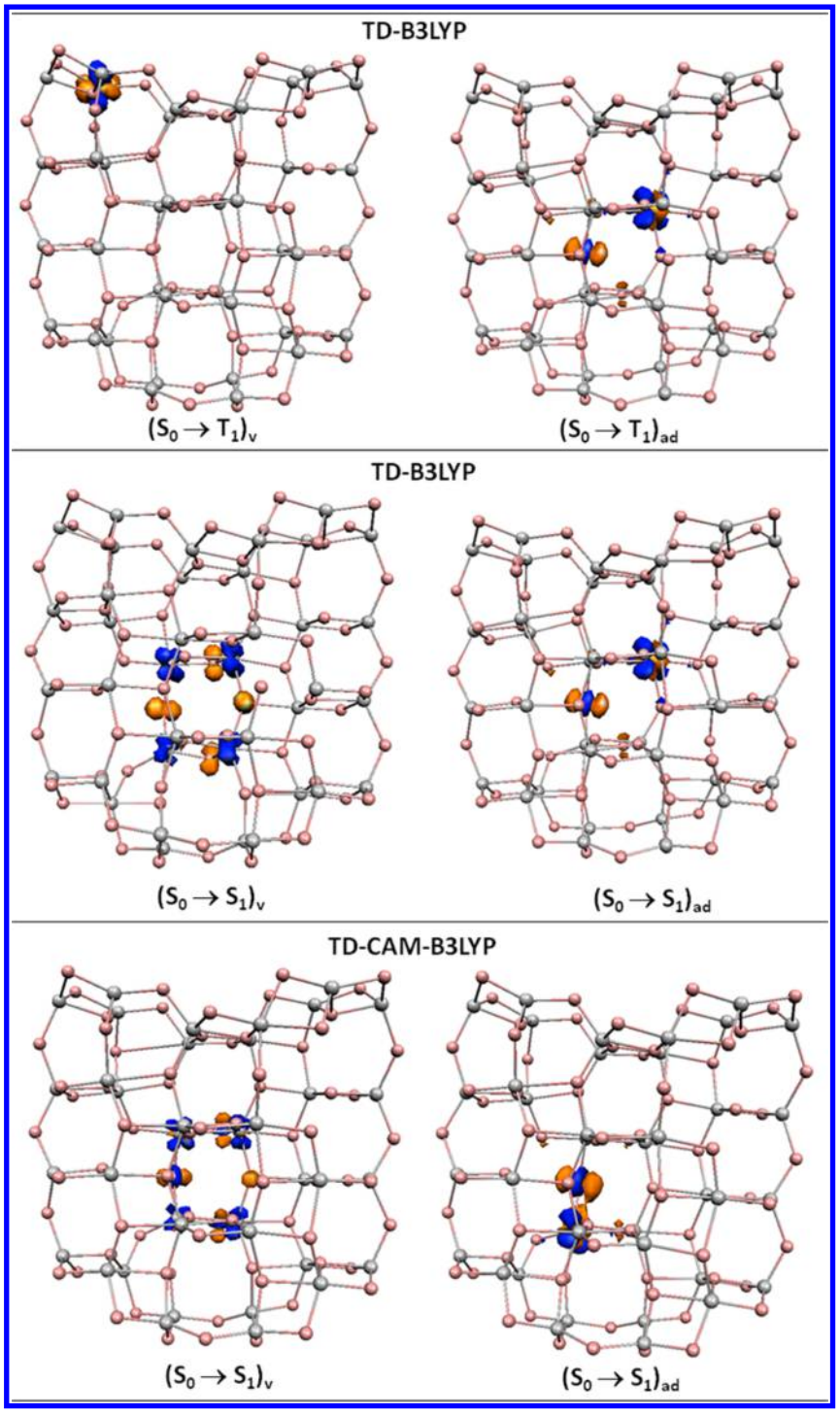

Figure 7. Density difference for the vertical (left side) and adiabatic (right side) lowest excitations (isovalue = 0.01 e/a.u.^{3}) computed in DMF solvent at the TD-B3LYP (singlet and triplet) and TD-CAM-B3LYP (singlet). Here, blue represents an electron density increase (i.e., where the excited electron of the photoexcited state is located), while orange represents a decrease in electron density upon excitation (i.e., where the hole is located).

density difference for the relaxed triplet (T_1) state at the TD-B3LYP level is similar to that for S_1, whereas in the vertical excitation the electron and hole are localized on a single undercoordinated Ti_{4c} center. By comparing the TD-B3LYP results in Figure 7 to the electron spin density computed at the SCF-B3LYP level (Figure 4), we can see a very similar localization for the excited electron and hole, while at the SCF-CAM-B3LYP level the charge carriers are localized on two Ti_{6c} and one O_{2c} centers more spatially separated than at the TD-CAM-B3LYP level, thus suggesting a more pronounced charge transfer character with respect to the TD-DFT approach.

4. CONCLUSIONS

In this work we have focused on the properties of trapped carriers in anatase TiO_2 NPs, which currently represent the materials of choice in photocatalysis and photovoltaics. We

DOI: 10.1021/ct500815x
J. Chem. Theory Comput. 2015, 11, 635−645

have investigated the structure and energetics of excitons and individual electron and hole polarons in a representative anatase TiO_2 NP by DFT calculations employing pure GGA (BLYP) and hybrid functionals with different HF-exc percentages (B3LYP-15, B3LYP, and the long-range corrected CAM-B3LYP functional). A difficult challenge inherently involved in the characterization of photoexcited TiO_2 NPs is the occurrence of many possible localization sites (local minima on the potential energy surface) for the photoexcited carriers. Remarkably, the surface truncation on small TiO_2 NPs (diameter <2 nm) gives rise to highly distorted structures with respect to the anatase bulk, rather resembling an amorphous TiO_2 structure.[32] The $(TiO_2)_{38}$ cluster employed in our calculations belongs to these small NPs, and, while in the initial configuration clearly retains the (101) surfaces, upon geometry optimization a highly distorted structure is attained. Therefore, the analysis of several different solutions is required for the photoexcited $(TiO_2)_{38}$ NP, especially in the case of higher HF-exc contribution. Altogether, however, our results indicate that the main trends do not depend significantly on the specific solution. Computed properties are found to depend significantly on the fraction of HF-exc, as well as on the introduction of long-range corrections. In particular, the two employed B3LYP and B3LYP-15 hybrid functionals yield self-trapping energies that differ by ∼0.26 eV for trapped electrons. The computed self-trapping energies for the $(TiO_2)_{38}$ NP at the B3LYP level of theory have values intermediate between anatase bulk and the (101) surface, as computed in ref 12 at the same level of theory. The protonated cluster $(TiO_2)_{38}H^+$ shows higher values for the self-trapping energies of the $(e^-\text{-}h^+)$ pair and of the single excess electron (0.09 and 0.21 eV, respectively) with respect to the $(TiO_2)_{38}$ NP at the same level of theory, in line with the possible trapping role of protonated oxygen sites in TiO_2. The solvent plays also a significant role in the trapping of the photoexcited carriers. Our results show that self-trapping energies are higher in vacuo than in DMF solvent by 0.1 eV for the T_1 exciton and excess electron states and by 0.3 eV for an excess hole. Moreover, the self-trapping energies of electron and hole polarons are found to be very similar in vacuo, whereas in both DMF and water solvents ΔE_{trap} values for the holes are 0.3−0.4 eV larger than for the electrons. Nevertheless, the MOs for the trapped electron (SOMO) and hole (SUMO) are almost at the same energy position inside the gap in vacuo, water, and DMF, even if the *absolute* energy values for electron and hole polaron states in DMF and water solvent differ by few eV with respect to vacuo.

We have also compared the performances of TD-DFT and SCF-DFT approaches for the description of the photoexcited polaron states in the stoichiometric $(TiO_2)_{38}$ cluster. The TD-CAM-B3LYP method nicely reproduces the experimental photoluminescence peak of self-trapped excitons, while the geometry optimized for the SCF T_1 state leads to a strong destabilization of the ground state, which substantially contributes to decrease the adiabatic SCF $(T_1 \rightarrow S_0)$ excitation energy. Therefore, TD-DFT employing range-separated functionals appears to provide a more realistic description of self-trapped exciton in anatase TiO_2 NPs.

Finally our study shows that the nanoscale size of the TiO_2 NPs gives rise to some significant differences in the structure and energetics of trapped charge carriers with respect to anatase bulk and extended surfaces. These results can help the interpretation of experimental results as well as the rationalization of the parameters controlling electron transport phenomena in TiO_2 materials, which is essential for the identification of strategies to reduce charge carrier recombination and enhance the charge collection efficiency in photovoltaic devices.

■ ASSOCIATED CONTENT

Supporting Information

Main geometrical and electronic parameters for the employed TiO_2 cluster computed at various level of theory both in vacuo, water, and DMF solvents. This material is available free of charge via the Internet at http://pubs.acs.org.

■ AUTHOR INFORMATION

Corresponding Authors

*E-mail: nunzi@thch.unipg.it.
*E-mail: filippo@thch.unipg.it.

Notes

The authors declare no competing financial interest.

■ ACKNOWLEDGMENTS

We thank FP7-ENERGY-2010 Project 261920 "ESCORT" and CNR-EFOR for financial support. A.S. thanks the support of DoE-BES, Chemical Sciences, Geosciences and Biosciences Division, Contract No. DE-FG02-12ER16286.

■ REFERENCES

(1) Mills, A.; Elliott, N.; Hill, G.; Fallis, D.; Durrant, J. R.; Willis, R. L. Preparation and characterisation of novel thick sol-gel titania film photocatalysts. *Photochem. Photobiol. Sci.* **2003**, *2*, 591−596.

(2) O'Regan, B.; Grätzel, M. A low-cost, high-efficiency solar cell based on dye-sensitized colloidal TiO_2 films. *Nature* **1991**, *353*, 737−740.

(3) (a) Yan, M. C.; Chen, F.; Zhang, J. L.; Anpo, M. Preparation of controllable crystalline titania and study on the photocatalytic properties. *J. Phys. Chem. B* **2005**, *109*, 8673−8678. (b) Wu, C. Y.; Yue, Y. H.; Deng, X. Y.; Hua, W. M.; Gao, Z. Investigation on the synergetic effect between anatase and rutile nanoparticles in gas-phase photocatalytic oxidations. *Catal. Today* **2004**, *93*−*5*, 863−869.

(4) (a) Forro, L.; Chauvet, O.; Emin, D.; Zuppiroli, L.; Berger, H.; Levy, F. High-mobility n-type charge-carriers in large single-crystals of anatse (TiO_2). *J. Appl. Phys.* **1994**, *75*, 633−635. (b) Frank, A. J.; Kopidakis, N.; van de Lagemaat, J. Electrons in nanostructured TiO2 solar cells: transport, recombination and photovoltaic properties. *Coord. Chem. Rev.* **2004**, *248*, 1165−1179.

(5) (a) Berger, T.; Sterrer, M.; Diwald, O.; Knözinger, E.; Panayotov, D.; Thompson, T. L.; Yates, J. T. Light-Induced Charge Separation in Anatase TiO_2 Particles. *J. Phys. Chem. B* **2005**, *109*, 6061−6068. (b) Chiesa, M.; Paganini, M. C.; Livraghi, S.; Giamello, E. Charge trapping in TiO_2 polymorphs as seen by Electron Paramagnetic Resonance spectroscopy. *Phys. Chem. Chem. Phys.* **2013**, *15*, 9435−9447. (c) Micic, O. I.; Zhang, Y. N.; Cromack, K. R.; Trifunac, A. D.; Thurnauer, M. C. Trapped holes on TiO_2 colloids studied by electron-paramagnetic-resonance. *J. Phys. Chem.* **1993**, *97*, 7277−7283. (d) Coronado, J. M.; Maira, A. J.; Conesa, J. C.; Yeung, K. L.; Augugliaro, V.; Soria, J. EPR study of the surface characteristics of nanostructured TiO_2 under UV irradiation. *Langmuir* **2001**, *17*, 5368−5374.

(6) (a) Knorr, F. J.; McHale, J. L. Spectroelectrochemical Photoluminescence of Trap States of Nanocrystalline TiO_2 in Aqueous Media. *J. Phys. Chem. C* **2013**, *117*, 13654−13662. (b) Tang, H.; Berger, H.; Schmid, P. E.; Levy, F. Optical- properties of anatase (TiO_2). *Solid State Commun.* **1994**, *92*, 267−271. (c) Katayama, I.; Watanabe, M.; Hayashi, T.; Tanaka, K. Photoexcited carrier dynamics in potassium tantalate. *J. Lumin.* **2005**, *112*, 242−245. (d) Preclikova, J.; Galar, P.; Trojanek, F.; Danis, S.; Rezek, B.; Gregora, I.; Nemcova,

DOI: 10.1021/ct500815x
J. Chem. Theory Comput. 2015, 11, 635−645

Y.; Maly, P. Nanocrystalline titanium dioxide films: Influence of ambient conditions on surface- and volume-related photoluminescence. *J. Appl. Phys.* **2010**, *108*, 113502. (e) Stevanovic, A.; Buttner, M.; Zhang, Z.; Yates, J. T. Photoluminescence of TiO_2: Effect of UV Light and Adsorbed Molecules on Surface Band Structure. *J. Am. Chem. Soc.* **2012**, *134*, 324−332.

(7) Thompson, T. L.; Yates, J. T. Monitoring hole trapping in photoexcited TiO_2(110) using a surface photoreaction. *J. Phys. Chem. B* **2005**, *109*, 18230−18236.

(8) Watanabe, M.; Hayashi, T. Time-resolved study of self-trapped exciton luminescence in anatase TiO_2 under two-photon excitation. *J. Lumin.* **2005**, *112*, 88−91.

(9) (a) Deskins, N. A.; Dupuis, M. Intrinsic Hole Migration Rates in TiO_2 from Density Functional Theory. *J. Phys. Chem. C* **2009**, *113*, 346−358. (b) Deskins, N. A.; Dupuis, M., Electron transport via polaron hopping in bulk TiO_2: A density functional theory characterization. *Phys. Rev. B* **2007**, *75*.

(10) (a) Finazzi, E.; Di Valentin, C.; Pacchioni, G.; Selloni, A. Excess electron states in reduced bulk anatase TiO_2: Comparison of standard GGA, GGA plus U, and hybrid DFT calculations. *J. Chem. Phys.* **2008**, *129*, 154113. (b) Di Valentin, C.; Pacchioni, G.; Selloni, A. Electronic structure of defect states in hydroxylated and reduced rutile TiO_2(110) surfaces. *Phys. Rev. Lett.* **2006**, *97*, 166803. (c) Yamamoto, T.; Ohno, T. A hybrid density functional study on the electron and hole trap states in anatase titanium dioxide. *Phys. Chem. Chem. Phys.* **2012**, *14*, 589−598.

(11) (a) Deskins, N. A.; Rousseau, R.; Dupuis, M. Localized Electronic States from Surface Hydroxyls and Polarons in TiO_2(110). *J. Phys. Chem. C* **2009**, *113*, 14583−14586. (b) Mattioli, G.; Filippone, F.; Alippi, P.; Bonapasta, A. A. Ab initio study of the electronic states induced by oxygen vacancies in rutile and anatase TiO_2. *Phys. Rev. B* **2008**, *78*, 241201(R).

(12) Di Valentin, C.; Selloni, A. Bulk and Surface Polarons in Photoexcited Anatase TiO_2. *J. Phys. Chem. Lett.* **2011**, *2*, 2223−2228.

(13) (a) Tomic, S.; Montanari, B.; Harrison, N. M. The group III-V's semiconductor energy gaps predicted using the B3LYP hybrid functional. *Phys. E* **2008**, *40*, 2125−2127. (b) Xiao, H.; Tahir-Kheli, J.; Goddard, W. A., III Accurate Band Gaps for Semiconductors from Density Functional Theory. *J. Phys. Chem. Lett.* **2011**, *2*, 212−217.

(14) Yanai, T.; Tew, D. P.; Handy, N. C. A new hybrid exchange-correlation functional using the Coulomb-attenuating method (CAM-B3LYP). *Chem. Phys. Lett.* **2004**, *393*, 51−57.

(15) Berardo, E.; Hu, H. S.; Shevlin, S. A.; Woodley, S. M.; Kowalski, K.; Zwijnenburg, M. A. Modeling Excited States in TiO_2 Nanoparticles: On the Accuracy of a TD-DFT Based Description. *J. Chem. Theory Comput.* **2014**, *10*, 1189−1199.

(16) Vittadini, A.; Selloni, A.; Rotzinger, F. P.; Gratzel, M. Structure and energetics of water adsorbed at TiO_2 anatase (101) and (001) surfaces. *Phys. Rev. Lett.* **1998**, *81*, 2954−2957.

(17) Lundqvist, M. J.; Nilsing, M.; Persson, P.; Lunell, S. DFT study of bare and dye-sensitized TiO_2 clusters and nanocrystals. *Int. J. Quantum Chem.* **2006**, *106*, 3214−3234.

(18) (a) De Angelis, F.; Tilocca, A.; Selloni, A. Time-dependent DFT study of $Fe(CN)_6^{4-}$ sensitization of TiO_2 nanoparticles. *J. Am. Chem. Soc.* **2004**, *126*, 15024−15025. (b) Persson, P.; Bergstrom, R.; Lunell, S. Quantum chemical study of photoinjection processes in dye-sensitized TiO_2 nanoparticles. *J. Phys. Chem. B* **2000**, *104*, 10348−10351.

(19) De Angelis, F.; Fantacci, S.; Selloni, A. Alignment of the dye's molecular levels with the TiO_2 band edges in dye-sensitized solar cells: a DFT-TDDFT study. *Nanotechnology* **2008**, *19*, 424002.

(20) De Angelis, F.; Fantacci, S.; Mosconi, E.; Nazeeruddin, M. K.; Gratzel, M. Absorption Spectra and Excited State Energy Levels of the N719 Dye on TiO_2 in Dye-Sensitized Solar Cell Models. *J. Phys. Chem. C* **2011**, *115*, 8825−8831.

(21) Sildos, I.; Kiisk, V.; Lange, S.; Aarik, J. Time-resolved exciton-emission spectroscopy of anatase. In *Advanced Organic and Inorganic Optical Materials*; Krumins, A., Millers, D., Muzikante, I., Sternbergs, A., Zauls, V., Eds.; Spie-Int Soc Optical Engineering: Bellingham, 2003; Vol. *5122*, pp 56−60.

(22) (a) Becke, A. D. Density-Functional exchange-energy approximation with correct asymptotic-behavior. *Phys. Rev. A* **1988**, *38*, 3098−3100. (b) Lee, C.; Yang, W.; Parr, R. G. Development of the Colle-Salvetti correlation-energy formula into a functional of the electron density. *Phys. Rev. B* **1988**, *37*, 785.

(23) (a) Becke, A. D. Density-Functionale thermochemistry 3. The role of exact exchange. *J. Chem. Phys.* **1993**, *98*, 5648−5652. (b) Stephens, P. J.; Devlin, F. J.; Chabalowski, C. F.; Frisch, M. J. Ab-initio calculation of vibrational absorption and circular-dichroism spectra using density-functional force-fields. *J. Phys. Chem.* **1994**, *98*, 11623−11627.

(24) (a) Reiher, M.; Salomon, O.; Hess, B. A. Reparameterization of hybrid functionals based on energy differences of states of different multiplicity. *Theor. Chem. Acc.* **2001**, *107*, 48−55. (b) Reiher, M. Theoretical study of the $Fe(phen)_2(NCS)_2$ spin-crossover complex with reparametrized density functionals. *Inorg. Chem.* **2002**, *41*, 6928−6935.

(25) Fouqueau, A.; Casida, M. E.; Daku, L. M. L.; Hauser, A.; Neese, F. Comparison of density functionals for energy and structural differences between the high-$[^5T_{2g}:(t_{2g})^4(e_g)^2]$ and low-$[^1A_{1g}:(t_{2g})^6(eg)^0]$ spin states of iron(II) coordination compounds. II. More functionals and the hexaminoferrous cation, $[Fe(NH_3)_6]^{2+}$. *J. Chem. Phys.* **2005**, *122*, 44110.

(26) Cossi, M.; Rega, N.; Scalmani, G.; Barone, V. Energies, Structures, and Electronic Properties of Molecules in Solution with the C-PCM Solvation Model. *J. Comput. Chem.* **2003**, *24*, 669−681.

(27) Frisch, M. J.; Trucks, G. W.; Schlegel, H. B.; Scuseria, G. E.; Robb, M. A.; Cheeseman, J. R.; Scalmani, G.; Barone, V.; Mennucci, B.; Petersson, G. A.; Nakatsuji, H.; Caricato, M.; Li, X.; Hratchian, H. P.; Izmaylov, A. F.; Bloino, J.; Zheng, G.; Sonnenberg, J. L.; Hada, M.; Ehara, M.; Toyota, K.; Fukuda, R.; Hasegawa, J.; Ishida, M.; Nakajima, T.; Honda, Y.; Kitao, O.; Nakai, H.; Vreven, T.; Montgomery, J. A., Jr.; Peralta, J. E.; Ogliaro, F.; Bearpark, M.; Heyd, J. J.; Brothers, E.; Kudin, K. N.; Staroverov, V. N.; Kobayashi, R.; Normand, J.; Raghavachari, K.; Rendell, A.; Burant, J. C.; Iyengar, S. S.; Tomasi, J.; Cossi, M.; Rega, N.; Millam, N. J.; Klene, M.; Knox, J. E.; Cross, J. B.; Bakken, V.; Adamo, C.; Jaramillo, J.; Gomperts, R.; Stratmann, R. E.; Yazyev, O.; Austin, A. J.; Cammi, R.; Pomelli, C.; Ochterski, J. W.; Martin, R. L.; Morokuma, K.; Zakrzewski, V. G.; Voth, G. A.; Salvador, P.; Dannenberg, J. J.; Dapprich, S.; Daniels, A. D.; Farkas, Ö.; Foresman, J. B.; Ortiz, J. V.; Cioslowski, J.; Fox, D. J. *Gaussian 09*, Revision A.1; Gaussian, Inc.: Wallingford CT, 2009.

(28) Dev, P.; Agrawal, S.; English, N. J. Functional Assessment for Predicting Charge-Transfer Excitations of Dyes in Complexed State: A Study of Triphenylamine-Donor Dyes on Titania for Dye-Sensitized Solar Cells. *J. Phys. Chem. A* **2013**, *117*, 2114−2124.

(29) Galynska, M.; Persson, P. Emerging Polymorphism in Nanostructured TiO_2: Quantum Chemical Comparison of Anatase, Rutile, and Brookite Clusters. *Int. J. Quantum Chem.* **2013**, *113*, 2611−2620.

(30) (a) Cramer, C. J.; Truhlar, D. G. Density functional theory for transition metals and transition metal chemistry. *Phys. Chem. Chem. Phys.* **2009**, *11*, 10757−10816. (b) Bredas, J.-L. Mind the gap! *Mater. Horiz.* **2014**, *1*, 17−19.

(31) Diebold, U. The surface science of titanium dioxide. *Surf. Sci. Rep.* **2003**, *48*, 53−229.

(32) Zhang, H. Z.; Banfield, J. F. Structural Characteristics and Mechanical and Thermodynamic Properties of Nanocrystalline TiO_2. *Chem. Rev.* **2014**, *114*, 9613−9644.

DOI: 10.1021/ct500815x
J. Chem. Theory Comput. 2015, 11, 635−645